Title

The myosin regulatory light chain Myl5 localizes to mitotic spindle poles and is required for proper cell division

Journal

Cytoskeleton, 78(2)

ISSN

1949-3584

Authors

Ramirez, Ivan
Gholkar, Ankur A
Velasquez, Erick F
et al.

Publication Date

2021-02-01

DOI

10.1002/cm.21654

Peer reviewed

HHS Public Access

Author manuscript

Cytoskeleton (Hoboken). Author manuscript; available in PMC 2022 March 08.

Published in final edited form as:

Cytoskeleton (Hoboken). 2021 February ; 78(2): 23–35. doi:10.1002/cm.21654.

The myosin regulatory light chain Myl5 localizes to mitotic spindle poles and is required for proper cell division

Ivan Ramirez[1], **Ankur A. Gholkar**[1], **Erick F. Velasquez**[1], **Xiao Guo**[1], **Bobby Tofig**[2], **Robert Damoiseaux**[2,3], **Jorge Z. Torres**[1,4,5,*]

[1]Department of Chemistry and Biochemistry, University of California, Los Angeles, CA 90095, USA

[2]California NanoSystems Institute, Los Angeles, CA 90095, USA

[3]Department of Molecular and Medical Pharmacology, Los Angeles, CA 90095, USA

[4]Molecular Biology Institute, University of California, Los Angeles, CA 90095, USA

[5]Jonsson Comprehensive Cancer Center, University of California, Los Angeles, CA 90095, USA

Abstract

Myosins are ATP-dependent actin-based molecular motors critical for diverse cellular processes like intracellular trafficking, cell motility, and cell invasion. During cell division, myosin MYO10 is important for proper mitotic spindle assembly, the anchoring of the spindle to the cortex, and positioning of the spindle to the cell mid-plane. However, myosins are regulated by myosin regulatory light chains (RLCs), and whether RLCs are important for cell division has remained unexplored. Here, we have determined that the previously uncharacterized myosin RLC Myl5 associates with the mitotic spindle and is required for cell division. We show that Myl5 localizes to the leading edge and filopodia during interphase and to mitotic spindle poles and spindle microtubules during early mitosis. Importantly, depletion of Myl5 led to defects in mitotic spindle assembly, chromosome congression, and chromosome segregation and to a slower transition through mitosis. Furthermore, Myl5 bound to MYO10 *in vitro* and co-localized with MYO10 at the spindle poles. These results suggest that Myl5 is important for cell division and that it may be performing its function through MYO10.

Keywords

Myl5; myosin light chain; mitosis; mitotic spindle; cell division

*Corresponding author: Jorge Z. Torres, 607 Charles E. Young Drive East, Los Angeles, CA 90095, Phone: 310-206-2092, Fax: 310-206-5213, torres@chem.ucla.edu.

AUTHOR CONTRIBUTIONS

I. R., X.G., E.F.V., A.A.G., B.T., R.D., and J.Z.T. contributed to the design, execution and analysis of experiments and data. I.R. and J.Z.T. wrote the manuscript with input and editing from all authors. All authors read and approved the final version of the manuscript.

1 | INTRODUCTION

The proper assembly of the bipolar mitotic microtubule spindle is critical to the fidelity of chromosome congression and segregation during cell division (Walczak and Heald 2008). During development, the anchoring and positioning of the mitotic spindle regulates the establishment of the cell division plane that is critical for cell fate determination (Morin and Bellaiche 2011). Important to mitotic spindle anchoring and positioning are astral microtubules that radiate out from the spindle poles and make contacts with the cell cortex (Nakajima 2018; di Pietro et al. 2016; Morin and Bellaiche 2011). Abnormal spindle assembly and orientation can result in defective cell divisions that can lead to developmental and proliferative diseases (Morin and Bellaiche 2011; di Pietro et al. 2016; Nakajima 2018). Although numerous components involved in assembling and orienting the spindle are known (Walczak and Heald 2008; Morin and Bellaiche 2011), the full complement of factors and the molecular signaling pathways that govern these events are not completely understood. Increasing evidence indicates that both the actin and microtubule cytoskeletal systems are necessary for proper cell division (Akhshi et al. 2014; Kita et al. 2019). Although actin has been highly studied within the context of interphase cells where it establishes the cellular architecture and regulates numerous important processes like cell motility, intracellular trafficking, cell signaling pathways, and gene expression (Hyrskyluoto and Vartiainen 2020; Moujaber and Stochaj 2020; Svitkina 2018; Titus 2018), less is known about its role during early cell division. However, actin has been shown to be critical for anchoring the spindle through microtubule-actin interactions at the cell cortex, for spindle positioning at the mid plane, and for actomyosin cellular constriction during cytokinesis (Akhshi et al. 2014; Thery and Bornens 2006; Uraji et al. 2018; Chaigne et al. 2016). Additionally, evidence indicates that an actin mesh assembly supports the bipolar meiotic and mitotic spindles, where actin provides rigidity and aids in focusing the spindle (Wuhr et al. 2008; Woolner et al. 2008; Mogessie and Schuh 2017; Kita et al. 2019). Therefore, actin plays an important role in ensuring the fidelity of cell division.

Myosins are ATP-dependent actin-based molecular motors that perform a variety of functions in muscle contraction, cargo transport, cell adhesion, and cell division; including spindle assembly, spindle orientation, and cytokinesis (Li et al. 2016; Hartman and Spudich 2012). During cell division, myosin-II is critical for acto-myosin ring contraction during cytokinesis, which is essential for bisecting one cell into two daughter cells (Murthy and Wadsworth 2005; Robinson and Spudich 2000). Of interest, the unconventional myosin-10 (MYO10) has been shown to be an important factor for establishing the architecture and function of the mitotic spindle through its binding to both actin and microtubules (Woolner et al. 2008; Wuhr et al. 2008; Sandquist et al. 2016; Weber et al. 2004; Kwon et al. 2015). MYO10 localizes to the spindle poles throughout mitosis and depletion of MYO10 leads to structural defects in the mitotic microtubule spindle, chromosome congression defects, and chromosome segregation defects (Woolner et al. 2008; Wuhr et al. 2008; Weber et al. 2004; Kwon et al. 2008). MYO10 also has important non-mitotic functions during interphase and in post-mitotic cells where it is important for filopodia formation and function (Sousa and Cheney 2005; Quintero and Yengo 2012; Kerber and Cheney 2011). The filopodia core is composed of actin filaments (Leijnse et al. 2015) and MYO10 has been shown

to be recruited to focal adhesions at the leading edge, undergoes intrafilopodial motility, accumulates at the filopodial tips, and promotes the formation and extension of filopodia (Tokuo et al. 2007; Berg and Cheney 2002; Bohil et al. 2006; Kerber et al. 2009; He et al. 2017; Sato et al. 2017). Therefore, myosins perform important functions that are necessary for cell division and cell motility.

The unconventional myosin holoenzymes typically consists of heavy and light chains (Li et al. 2016). Myosin light chains are required for the structural integrity of the myosin holoenzyme and have regulatory functions on the activity of the protein complex (Li et al. 2016; Heissler and Sellers 2016; Heissler and Sellers 2014). There are two major groups of myosin light chains, the Essential Light Chains (ELCs) and the Regulatory Light Chains (RLCs) (Heissler and Sellers 2016; Heissler and Sellers 2014). The ELCs are essential for the enzymatic activity of the myosin and removal or depletion of the ELCs from the myosin leads to a dramatic loss of myosin enzymatic activity (Heissler and Sellers 2016; Heissler and Sellers 2014). The RLCs are involved in regulating the enzymatic activity of the myosin and their removal or depletion typically leads to moderate effects on myosin activity (Heissler and Sellers 2016; Heissler and Sellers 2014). For example, both calmodulin (CaM) and calmodulin-like protein (CLP) have been shown to be MYO10 light chains that regulate MYO10 motility and function (Homma et al. 2001; Bennett et al. 2007; Bennett et al. 2008; Rogers and Strehler 2001). Although myosin-II and MYO10 have important roles in cell division, the role of RLCs (if any) in cell division has remained unexplored.

We recently performed a microscopy-based RNAi screen using an siRNA library (25,620 siRNAs) targeting the druggable genome in HeLa cells, that included enzymes like kinases and components of molecular motors like myosins, to identify novel factors whose depletion led to a slowed cell division (Torres lab unpublished). This screen identified 13 novel proteins that were not known to be important for cell division, among which was myosin light chain 5 (Myl5). Although Myl5 has remained poorly characterized, based on its protein sequence similarity it is predicted to be a myosin RLC (Collins et al. 1992). Dysregulation of *MYL5* mRNA levels has been observed in glioblastoma multiforme, cervical carcinoma, and breast cancer (Zhang et al. 2017; Alshabi et al. 2019; Savci-Heijink et al. 2019). For example, *MYL5* mRNA levels are upregulated in late stage cervical cancer patients and is associated with poor survival (Zhang et al. 2017). Additionally, *MYL5* overexpression promoted tumor cell metastasis in a cervical cancer mouse model (Zhang et al. 2017). Here, we have discovered that Myl5 is important for mitotic spindle assembly, chromosome congression, and proper cell division. GFP-Myl5 localizes to the spindle poles during mitosis, indicating that its localization is cell cycle phase dependent. GFP-Myl5 co-localized with spindle pole proteins and MYO10 and bound to MYO10 *in vitro*. Importantly, depletion of Myl5 led to spindle assembly defects, chromosome congression defects, and chromosome segregation errors. These results suggest that Myl5 has important roles in spindle assembly and chromosome segregation and that it may be performing its function through its association with MYO10.

2 | RESULTS AND DISCUSSION

2.1 | *In silico* analysis of Myl5

Our recent genetic RNAi screen for novel cell division proteins led us to discover myosin light chain 5 (Myl5), an uncharacterized hypothetical myosin regulatory light chain (RLC) of the MLC2 type. Human Myl5 is a 173 amino acid protein with 3 EF hand domains predicted to be important for calcium binding in other myosin regulatory light chains (Figure 1a) (Heissler and Sellers 2014; Grabarek 2006). A phylogenetic tree (Hunt et al. 2018) analysis indicated that Myl5 was conserved among vertebrates (Figure 1b). An Online Mendelian Inheritance in Man (OMIM) search showed that the *MYL5* gene was within the 4p16.3 region where the Huntington Disease locus is located. However, *MYL5* has not been linked to inherited human diseases. Due to recent studies showing the upregulation of *MYL5* expression in cervical cancer (Zhang et al. 2017) and the down regulation of *MYL5* expression in breast (Savci-Heijink et al. 2019) and brain cancers (Alshabi et al. 2019), we sought to determine if *MYL5* was widely dysregulated in other types of cancers. Interestingly, analysis of *MYL5* and *MYO10* differential gene expression across a broad array of cancers using the Gene Expression Profiling and Interactive Analysis (GEPIA) web server (Tang et al. 2017) showed that *MYL5* mRNA levels were lower in most cancers compared to matched normal samples, whereas *MYO10* mRNA levels were elevated in most cancers compared to normal samples (Figure 1c). Additionally, a GEPIA survival analysis showed that low *MYL5* mRNA levels and high *MYO10* mRNA levels related to an unfavorable overall survival (Figure 1d). Together, these analyses showed that the Myl5 protein is conserved among vertebrates and that *MYL5* and *MYO10* gene expression is widely dysregulated in cancer.

2.2 | Myl5 localizes to the spindle poles and spindle microtubules during cell division

Although previous genomic and bioinformatic studies had implicated Myl5 in myosin related functions and in tumorigenesis, its biological function had remained poorly characterized. To begin to understand the cellular role of Myl5 and its link to tumorigenesis, we analyzed its subcellular localization throughout the cell cycle. First, we generated a LAP(GFP-TEV-S-Peptide)-Myl5 inducible stable cell line that expressed GFP-Myl5 upon induction with Dox (Figure S1a) (Torres et al. 2009; Bradley et al. 2016). The LAP-Myl5 cell line was treated with Dox for 16 hours to express GFP-Myl5 and cells were fixed, stained with Hoechst 33342 DNA dye, and anti-α-Tubulin and anti-GFP antibodies and imaged by immunofluorescence microscopy. During interphase GFP-Myl5 was dispersed throughout the nucleus and cytoplasm of the cell (Figure 2a). Interestingly, GFP-Myl5 localized to the spindle poles in early mitosis, and to a lesser extent the mitotic spindle, and remained associated with the poles until mitotic exit (Figure 2a). To further define the GFP-Myl5 subcellular localization in early mitosis, we performed immunofluorescence co-localization studies with centrosome and spindle pole markers. The GFP-Myl5 localization signal overlapped with NUMA at the spindle poles and encompassed the Pericentrin and Centrin signals, which stained the centrosomes (Figure 2b,c; Figure S1b). Furthermore, in cells with high levels of GFP-Myl5 expression, GFP-Myl5 also co-localized with TPX2 on the spindle microtubules (Figure S1c). Due to the change in GFP-Myl5 localization at mitotic entry, we next asked if endogenous Myl5 protein levels were also cell cycle

regulated. HeLa cells were synchronized in G1/S with thymidine treatment, released into the cell cycle, cells were harvested every hour, and protein extracts were prepared. Immunoblot analysis of these samples with anti-Myl5 and anti-Cyclin B antibodies indicated that endogenous Myl5 protein levels remained steady in G1/S and G2/M and decreased slightly during mitotic exit, a time when mitotic Cyclin B levels decreased (Figure 2d). Additionally, the anti-Myl5 antibody recognized two protein bands that corresponded with the size of the two Myl5 isoforms (19.5 kD, UniProtKB-Q02045-1; 14.9 kD, UniProtKB-Q02045-2). Together, these results indicated that the Myl5 protein is abundant throughout the cell cycle and that it undergoes a dynamic cell cycle dependent change in subcellular localization where it redistributes from the nucleus and cytoplasm in interphase to the spindle poles during mitotic entry and remains associated with the poles throughout mitosis.

2.3 | Myl5 is required for proper cell division

Next, we asked if Myl5 was required for cell division by depleting Myl5 in HeLa cells. First, we sought to identify siRNA oligonucleotides which reduced Myl5 protein levels to less than 10% compared to non-targeting control siRNA. HeLa cells were transfected with non-targeting control siRNA (siCtrl) or siRNAs targeting Myl5 (siM1-siM4) for 72 hours and cell lysates were prepared and analyzed by immunoblotting. The siM1-siM4 oligonucleotides depleted Myl5 protein levels to undetectable levels (Figure 3a; Figure S2a). Next, we sought to analyze the consequences of depleting Myl5 protein levels during cell division. HeLa cells were transfected with siCtrl or siM1-siM4 siRNAs for 72 hours. The cells were then fixed and co-stained with Hoechst 33342 (to visualize the DNA) and anti-α-Tubulin antibodies to detect the mitotic microtubule spindle. Interestingly, depletion of Myl5 led to a significant increase in cells with a defective mitosis, including an increase in the percentage of prometaphase cells with multipolar spindles (siM1= 20.75±3.59%, p=.0004 compared to siCtrl= 7.5±1.29%) and anaphase cells with lagging chromosomes (siM1= 32.25±2.5%, p<.0001 compared to siCtrl= 8.25±3.1%) (Figure 3b–e; Figure S2b–f). Importantly, the mitotic defects (multipolar spindles and lagging chromosomes) observed upon siM1 treatment were rescued with the expression of a siRNA-resistant (siRes) version of GFP-Myl5 (for multipolar spindles- siM1+ GFP-Myl5-siRes= 3.0±1.0%, p=.0270 compared to siM1+ GFP-Myl5-WT= 8.33±2.51%; for lagging chromosomes- siM1+ GFP-Myl5-siRes= 9.67±1.5%, p=.0026 compared to siM1+ GFP-Myl5-WT= 19.67±2.08%) (Figure 3f,g; Figure S3). Together, these results indicated that Myl5 was required for proper cell division and that its depletion led to cell division errors.

2.4 | The levels of Myl5 affect the timing of cell division

Next, we asked if the overall time to cell division was affected by the depletion of Myl5. HeLa cells were transfected with non-targeting control siRNA (siCtrl) or siRNAs targeting Myl5 (siM1 and siM3) for 48 hours, synchronized in G1/S with thymidine treatment for 18 hours, and released in media containing the cell permeable DNA specific stain SiR-DNA (visible in the far-red channel). Five-hours post release live cells were imaged at 20X magnification at five-minute intervals for 18 hours. Movies were then analyzed and the time from nuclear DNA condensation to nuclear separation was quantified. This analysis showed that depletion of Myl5 led to a significant increase in the time that cells spent in mitosis with the average time from nuclear DNA condensation to nuclear separation for siM1= 55±27.4

minutes (p<.0001) and siM3 = 46±22 minutes (p=.0288) compared to siCtrl= 38.9±21.6 minutes (Figure 4a,b; Supporting Videos S1–S3).

2.5 | Myl5 binds MYO10 and colocalizes with MYO10 to the spindle poles

Due to the ability of MYO10 to localize to the spindle poles in early mitosis and its functional importance in ensuring the fidelity of spindle assembly, chromosome congression, chromosome segregation, and cell division (Woolner et al. 2008), we asked if Myl5 and MYO10 shared a similar localization during mitosis. The LAP-Myl5 cell line was used to express GFP-Myl5 and cells were fixed, stained with Hoechst 33342 DNA dye, and anti-α-Tubulin, anti-MYO10, and anti-GFP antibodies and imaged by immunofluorescence microscopy. Indeed, the GFP-Myl5 and MYO10 localization signals overlapped at the spindle poles throughout mitosis (Figure 5a). Next, we sought to determine if Myl5 and MYO10 could associate directly. *In vitro* binding experiments were performed with HA-Myl5 and FLAG-GFP or FLAG-MYO10. Indeed, MYO10 co-immunoprecipitated with Myl5 (Figure 5b). The IQ motifs of myosins are key sites for binding to regulatory light chains (Heissler and Sellers 2014), thus we asked if the IQ motifs of MYO10 were necessary for the MYO10-Myl5 interaction. To do this, we removed the three IQ motifs from MYO10 to generate MYO10 IQ-less (MYO10-IQL). *In vitro* binding experiments with HA-Myl5 or HA-CALM3 (Calmodulin 3, a known MYO10 regulatory light chain that binds to the MYO10 IQ motifs (Rogers and Strehler 2001)) and FLAG-GFP, FLAG-MYO10, or FLAG-MYO10-IQL showed that Myl5 was able to bind to both MYO10 and MYO10-IQL, while CALM3 only bound to MYO10 and not MYO10-IQL (Figure 5c,d; Figure S4). Together, these data indicated that Myl5 binds to MYO10, independent of the IQ motifs, and colocalizes with MYO10 at the spindle poles during mitosis.

2.6 | Myl5 localizes to the leading edge of the cell and to filopodia in interphase cells

Within the context of cancer, actin-based structures like filopodia are critical for cell migration, invasion, and metastasis (Caswell and Zech 2018; Jacquemet et al. 2015). Of interest, MYO10 has a critical role in filopodia formation and accumulates at the tips of filopodia (Bohil et al. 2006; Tokuo et al. 2007; Kerber et al. 2009) and has been linked to promoting cancer invasion and metastasis, including in breast cancer and melanomas (Arjonen et al. 2014; Courson and Cheney 2015; Tokuo et al. 2018; Cao et al. 2014). Due to the association of Myl5 with MYO10, we sought to determine whether Myl5 also localized to filopodia like MYO10. The LAP-Myl5 or LAP-MYO10 cell lines was used to express GFP-Myl5 or GFP-MYO10 and cells were fixed, stained with Hoechst 33342 DNA dye, anti-α-Tubulin, anti-Fascin (marker for filopodia (Edwards and Bryan 1995; Otto et al. 1979)), and anti-GFP antibodies and imaged by immunofluorescence microscopy. Interestingly, GFP-Myl5 localized to the leading edge of the cell and throughout filopodia, but did not accumulate at the tips of filopodia like MYO10 (Figure 6a). Calcium binding and phosphorylation are two key mechanisms for regulating myosin RLC function (Heissler and Sellers 2016). RLCs typically have multiple EF hands that are generally thought bind calcium, however, only EF hands with a calcium binding consensus pattern of amino acids are predicted to have the ability to bind calcium (prosite prorule annotation rule: PRU00448, (Sigrist et al. 2005)) (Grabarek 2006). Specifically, Myl5 has three EF-hands, but only the N-terminal EF-hand contains the calcium binding consensus (amino acids 43–54) (Figure

1a). Additionally, RLCs are typically phosphorylated at consensus Ser/Thr residues in their N-terminus, which are conserved in Myl5 (Figure S5) (Yu et al. 2016). Therefore, we sought to determine whether deletion of the predicted Myl5 calcium binding site or mutation of the conserved RLC sites of phosphorylation (serines 20 and 21, Figure S5) would perturb the localization of GFP-Myl5 to cytoskeletal structures. To do this, we generated LAP-tagged inducible stable cell lines of Myl5 calcium binding site deletion (CAD), phospho-null (20A and 21A (AA)) and phospho-mimic (20E or 21E) mutants; although phospho-mimetic mutants in other RLCs do not always have the anticipated effect on myosin activity (Heissler and Sellers 2015; Vasquez et al. 2016). Immunofluorescence microscopy of HeLa cells overexpressing these GFP-Myl5 mutants, showed that they were capable of localizing to the leading edge, filopodia, and the spindle poles, similar to wild type GFP-Myl5 (Figure 6b–e). Additionally, no major perturbations to the overall architecture of filopodia, spindles, and spindle poles were observed by the overexpression of these Myl5 mutants. Together, these results showed that GFP-Myl5 localizes to the leading edge and filopodia during interphase and that conserved residues in Myl5 that regulate the function of other RLCs are not required for its localization to these structures.

2.7 | CONCLUSION

Although actin and the unconventional myosin MYO10 had been implicated in ensuring the fidelity of mitotic spindle assembly and cell division, the role of myosin RLCs during cell division remained unknown. Here, we have determined that Myl5 is a novel and important factor necessary for proper cell division. GFP-Myl5 localized to the leading edge and filopodia in interphase cells and to the spindle poles and spindle microtubules during early mitosis. Depletion of Myl5 led to mitotic spindle defects, errors in chromosome congression and segregation, and a slowed progression through mitosis. These Myl5 depletion phenotypes were similar to those reported upon MYO10 depletion (Woolner et al. 2008), albeit less severe. Interestingly, the GFP-Myl5 immunofluorescence signal overlapped with MYO10 at the spindle poles throughout mitosis and Myl5 bound directly to MYO10 *in vitro*. Our results suggest that Myl5 is important for cell division and that it may function through MYO10. To our knowledge, Myl5 is the first myosin RLC family member that has been implicated in mitotic spindle assembly.

Of the ~40 myosins encoded in the human genome, at least ten (including MYO10) have been implicated in tumorigenesis (Li and Yang 2016). Our analysis showing that *MYL5* and *MYO10* gene expression are frequently dysregulated in cancer compared to normal samples is intriguing and puzzling. While *MYL5* mRNA levels were lower in most cancers and related to unfavorable survival, *MYO10* mRNA levels were elevated in most cancers and related to unfavorable survival (Figure 1c,d). These results are consistent with reports showing low levels of *MYL5* mRNA in breast (Savci-Heijink et al. 2019) and brain cancers (Alshabi et al. 2019) and high *MYO10* mRNA levels in invasive and metastatic breast cancer and melanoma (Arjonen et al. 2014; Courson and Cheney 2015; Tokuo et al. 2018; Cao et al. 2014). However, others have reported that *MYL5* mRNA levels are elevated in late stage cervical cancer patients, are associated with poor survival, and can promote tumor cell metastasis in mouse models of cervical cancer (Zhang et al. 2017). Similarly, the upregulation of *MYO10* mRNA levels in invasive and metastatic cancers is consistent with

its critical role in promoting filopodia formation, which are important for cell motility and invasion (Tokuo et al. 2007; Berg and Cheney 2002; Bohil et al. 2006; Kerber et al. 2009; He et al. 2017; Sato et al. 2017; Caswell and Zech 2018; Jacquemet et al. 2015). However, it is the depletion of MYO10 that leads to cell division defects and genetic instability (Woolner et al. 2008; Wuhr et al. 2008; Weber et al. 2004; Kwon et al. 2008) and what role this may play in early stage cancers remains to be determined. Therefore, it is possible that *MYL5* and *MYO10* mRNA levels are differentially expressed in early versus late stage tumors and further research in this area is warranted. Although our data suggest that Myl5 may be affecting cell division through MYO10, it is possible that Myl5 may function independently or with other non-motor proteins. We also note that during interphase, myosin light chains have been implicated in regulating gene expression by binding to specific sequences within the promoter region of target genes (Zhang et al. 2015; Li and Sarna 2009) and that Myl5 has been shown to bind the promoter region of HIF-1alpha, an important factor in tumorigenesis, and regulates its expression (Rankin and Giaccia 2016; Zhang et al. 2017). Consistent with this function, GFP-Myl5 localized to both the cytoplasm and nucleus in interphase cells (Figure 6a). Therefore in addition to its cytoskeleton-related function, Myl5 has cytoskeleton unrelated functions in gene expression that may contribute to tumorigenesis.

3 | MATERIALS and METHODS

3.1 | Cell culture

HeLa cells were grown in F12:DMEM 50:50 (Hyclone) with 10% FBS, 2mM L-glutamine and antibiotics in 5% CO_2 at 37 °C. Cells were synchronized in G1/S by treatment with 2 mM thymidine (Sigma-Aldrich) for 18-hours. The following siRNAs were used for siRNA transfections: ThermoFisher Silencer Select 4390843 (control non-targeting siRNA) and S9187 and S9188 (M1 and M2 siRNAs targeting *MYL5*); Dharmacon ON-TARGETplus D-001810-10 (control non-targeting siRNA) and J-011739-03 and J-011739-04 (M3 and M4 siRNAs targeting *MYL5*) were used as described previously (Torres et al. 2010). See Table S1 for a list of key reagents and resources used in this study and their pertinent information.

3.2 | Generation of the LAP-Myl5 inducible stable cell line

The HeLa LAP(GFP-TEV-S-Peptide)-Myl5, -Myl5-AA, -Myl5-20E, -Myl5-21E, -Myl5-CAD, -Myl5-siRes, and -MYO10 inducible stable cell lines were generated as described previously (Torres et al. 2009; Bradley et al. 2016). Briefly, full-length *MYL5* (coding for amino acid residues 1–173) and mutant derivatives (alanine mutations at both Ser20 and Ser21 (AA); Glu mutations at either Ser20 (20E) or Ser21 (21E); deletion of the calcium binding domain (amino acids 43–54, CAD)) and full-length MYO10 (coding for amino acid residues 1–2058) were cloned into pDONR221 and transferred to pGLAP1 through a Gateway reaction to generate the pGLAP1 vectors with these ORFs that were transfected into HeLa Flp-In T-Rex cells to generate their respective inducible stable cell lines.

3.3 | Immunoblotting

For Myl5 cell cycle protein expression analysis, HeLa cells were synchronized in G1/S with 2 mM thymidine for 18-hours. Cells were then washed with PBS three times and twice with

F12:DMEM media with 10% FBS and released into the cell cycle. Cells were harvested at the indicated time points, lysed, and protein extracts were resolved on a 4–20% SDS-PAGE and transferred to a PVDF membrane. The membranes were immunoblotted with the indicated antibodies and imaged with a LiCOR system. The same approach was used to detect Myl5 protein depletion upon siRNA transfections without the cell synchronization step. Cell extract preparation and immunoblot analyses with the indicated antibodies were as described previously (Gholkar et al. 2016).

3. 4 | Fixed-cell immunofluorescence microscopy and live-cell time-lapse microscopy

Fixed-cell immunofluorescence microscopy was performed as described previously (Gholkar et al. 2016). Briefly, non-transfected cells or cells that had been transfected with the indicated siRNAs for 48 hours were arrested in G1/S with 2 mM thymidine for 18 hours, washed, and released into fresh media for eight hours. Cells were then fixed with 4% paraformaldehyde, permeabilized with 0.2% Triton X-100/PBS, and co-stained with 0.5 μg/ml Hoechst 33342 (ThermoFisher) to visualize the DNA and the indicated antibodies. A Leica DMI6000 microscope (Leica DFC360 FX Camera, 63x/1.40–0.60 NA oil objective, Leica AF6000 software) was then used to capture the images, which were deconvolved with the Leica Application Suite 3D Deconvolution software and exported as TIFF files. For quantifying mitotic defects, the data from four independent experiments, with 100 cells counted for each, was used to quantify the average ± standard deviation (SD). For time-lapse microscopy, HeLa cells were transfected with the indicated siRNAs for 48 hours, arrested in G1/S with 2 mM thymidine for 18 hours, washed, and released into fresh media containing 100 nM SiR-DNA stain (Cytoskeleton Inc.). Cells were imaged live five-hours post release for 18 hours using an ImageXpress XL imaging system (Molecular Devices) with a 20x air objective at 37 °C in 5% CO_2. Captured images were exported as a video at one half frames per second using Image J and the videos were saved as AVI movies. Each frame represents a five-minute interval. For quantifying the timing of cell division, the data from three independent experiments, with 30 cells counted for each, was used to quantify the average time in minutes from DNA condensation for nuclear separation ± standard deviation (SD).

3.4.1 | Statistical analysis—All statistical data are presented as the average ± SD from at least three independent experiments. Outliers were considered in time-lapse experiments by using Tukey's method in R (https://www.r-project.org/). For experiments where two groups were compared, they were analyzed using unpaired Student's t test. Data was judged to be statistically significant when $p < 0.05$. For experiments where three or more groups were compared, they were first tested for significance using ANOVA statistical test. If p-value showed significance ($p < 0.05$), multiple pair-wise comparisons were performed between the means of groups using Tukey Honest Significant Difference and Dunnet's tests. All statistical figures were generated with GraphPad Prism 5.

3.5 | Generation of plasmids and *in vitro* binding assays

For *in vitro* binding assays, full-length human *MYL5* (encoding amino acid residues 1–173) or *CALM3* (encoding amino acid residues 1–149) were fused to the C-terminus of the HA-tag to generate the pCS2-HA-*MYL5* and pCS2-HA-*CALM3* vectors. Similarly

full-length *MYO10* (encoding amino acid residues 1–2058) or *MYO10* lacking amino acids 742–817 that contain the IQ motifs (*MYO10-IQL*) were fused to the C-terminus of the FLAG-tag to generate the pCS2-FLAG-*MYO10* and pCS2-FLAG-*MYO10-IQL* vectors. *In vitro* binding assays were performed as described previously (Gholkar et al. 2016). Briefly, HA-Myl5, HA-CALM3, FLAG-MYO10, FLAG-MYO10-IQL, and FLAG-GFP (negative control) were *in vitro* transcribed and translated (IVT) using TNT® Quick Coupled Transcription/Translation System, (Promega) in 10 μL reactions. Magnetic HA beads (MBL International) were washed three times and equilibrated with wash buffer (50 mM Tris pH 7.4, 200 mM KCl, 1 mM DTT, 0.5% NP-40, and Halt Protease and Phosphatase Inhibitor Cocktail). IVT reactions were added to the equilibrated HA beads and incubated for 1.5 hours at 30 °C with gentle shaking. Beads were washed three times with wash buffer and eluted by boiling for five minutes with 2X Laemmli SDS sample buffer. Samples were resolved on a 4–20% gradient Tris gel with Tris-Glycine SDS running buffer, transferred to an Immobilon PVDF membrane (EMD Millipore), and membranes were analyzed with a PharosFX Plus molecular imaging system (Bio-Rad).

3.6 | *In silico* analysis of Myl5

The Myl5 phylogenetic tree was constructed by querying Ensembl (Hunt et al. 2018) (https://www.ensembl.org/) for Myl5 (ID: ENSGT00940000163023) and Figure 1b was generated by reconstructing the phylogenetic tree on Ensembl using images from LogoMarkr (https://logomakr.com/). For analysis of *MYL5* and *MYO10* differential gene expression in cancer cells compared to normal counterparts, their gene expression profiles were retrieved from the Gene Expression Profiling Interactive Analysis (GEPIA), an interactive web server for cancer genomics that compares cancer and normal gene expression (Tang et al., 2017). For a list of cancer types considered and their corresponding abbreviations refer to Table S2. The median gene expression for both tumor and matched normal samples were compared by subtracting median normal from tumor gene expression for each cancer type. Positive values represent higher gene expression in tumor samples compared to normal samples and negative values represent lower gene expression in tumor samples compared to normal samples. Figure 1c summarizes the gene expression compared to normal samples in different tumor types for both *MYL5* and *MYO10*. Correlation analysis between *MYL5* and *MYO10* mRNA levels and the overall survival of cancer patients was carried out using the Survival Plot tool in GEPIA with default parameters. Datasets for all cancers and matched normal samples listed on Table S2 were used in the analysis. Survival plots were exported as PDF files.

3.7 | Antibodies

Immunofluorescence and immunoblotting were carried out using antibodies against: Myl5, MYO10, and Fascin (Proteintech: 14249-1-AP, 24565-1-AP, and 66321-1-lg); Pericentrin (Novus Biologicals: NB-100-68277); GFP (Abcam: ab13970); Gapdh (GTX100118); α-Tubulin (Bio-Rad: MCA78G); Cyclin B (Santa Cruz: sc-245). Centrin antibodies were a gift from J. Salisbury and NUMA and TPX2 antibodies were gifts from D. Compton. Secondary antibodies conjugated to FITC, Cy3, and Cy5 were from Jackson Immuno Research and those conjugated to IRDye 680 and IRDye 800 were from LI-COR Biosciences.

Supplementary Material

Refer to Web version on PubMed Central for supplementary material.

ACKNOWLEDGMENTS

This material is based upon work supported by the National Science Foundation under Grant Number MCB1912837 to J.Z.T., any opinions, findings, and conclusions or recommendations expressed in this material are those of the authors and do not necessarily reflect the views of the National Science Foundation. This work was supported in part by a grant to The University of California, Los Angeles from the Howard Hughes Medical Institute through the James H. Gilliam Fellowships for Advanced Study program to E.F.V. This work was also supported by an NSF Louis Stokes Alliances for Minority Participation Bridge to the Doctorate Fellowship and Cota Robles Fellowship to I.R. Work performed in the UCLA Molecular Screening Shared Resource was supported by the National Cancer Institute of the National Institutes of Health under award number P30CA016042

DATA AVAILABILITY STATEMENT

The data that support the findings of this study are available from the corresponding author upon request.

REFERENCES

Akhshi TK, Wernike D and Piekny A. 2014. Microtubules and actin crosstalk in cell migration and division. Cytoskeleton (Hoboken) 71(1):1–23. [PubMed: 24127246]

Alshabi AM, Vastrad B, Shaikh IA and Vastrad C. 2019. Identification of Crucial Candidate Genes and Pathways in Glioblastoma Multiform by Bioinformatics Analysis. Biomolecules 9(5).

Arjonen A, Kaukonen R, Mattila E, Rouhi P, Hognas G, Sihto H, Miller BW, Morton JP, Bucher E, Taimen P et al. 2014. Mutant p53-associated myosin-X upregulation promotes breast cancer invasion and metastasis. J Clin Invest 124(3):1069–82. [PubMed: 24487586]

Bennett RD, Mauer AS and Strehler EE. 2007. Calmodulin-like protein increases filopodia-dependent cell motility via up-regulation of myosin-10. J Biol Chem 282(5):3205–12. [PubMed: 17130134]

Bennett RD, Caride AJ, Mauer AS and Strehler EE. 2008. Interaction with the IQ3 motif of myosin-10 is required for calmodulin-like protein-dependent filopodial extension. FEBS Lett 582(16):2377–81. [PubMed: 18570893]

Berg JS and Cheney RE. 2002. Myosin-X is an unconventional myosin that undergoes intrafilopodial motility. Nat Cell Biol 4(3):246–50. [PubMed: 11854753]

Bohil AB, Robertson BW and Cheney RE. 2006. Myosin-X is a molecular motor that functions in filopodia formation. Proc Natl Acad Sci U S A 103(33):12411–6. [PubMed: 16894163]

Bradley M, Ramirez I, Cheung K, Gholkar AA and Torres JZ. 2016. Inducible LAP-tagged Stable Cell Lines for Investigating Protein Function, Spatiotemporal Localization and Protein Interaction Networks. J Vis Exp 118(118):54870.

Cao R, Chen J, Zhang X, Zhai Y, Qing X, Xing W, Zhang L, Malik YS, Yu H and Zhu X. 2014. Elevated expression of myosin X in tumours contributes to breast cancer aggressiveness and metastasis. Br J Cancer 111(3):539–50. [PubMed: 24921915]

Caswell PT and Zech T. 2018. Actin-Based Cell Protrusion in a 3D Matrix. Trends Cell Biol 28(10):823–34. [PubMed: 29970282]

Chaigne A, Campillo C, Voituriez R, Gov NS, Sykes C, Verlhac MH and Terret ME. 2016. F-actin mechanics control spindle centring in the mouse zygote. Nat Commun 7:10253. [PubMed: 26727405]

Collins C, Schappert K and Hayden MR. 1992. The genomic organization of a novel regulatory myosin light chain gene (MYL5) that maps to chromosome 4p16.3 and shows different patterns of expression between primates. Hum Mol Genet 1(9):727–33. [PubMed: 1284596]

Courson DS and Cheney RE. 2015. Myosin-X and disease. Exp Cell Res 334(1):10–5. [PubMed: 25819274]

di Pietro F, Echard A and Morin X. 2016. Regulation of mitotic spindle orientation: an integrated view. EMBO Rep 17(8):1106–30. [PubMed: 27432284]

Edwards RA and Bryan J. 1995. Fascins, a family of actin bundling proteins. Cell Motil Cytoskeleton 32(1):1–9. [PubMed: 8674129]

Gholkar AA, Senese S, Lo YC, Vides E, Contreras E, Hodara E, Capri J, Whitelegge JP and Torres JZ. 2016. The X-Linked-Intellectual-Disability-Associated Ubiquitin Ligase Mid2 Interacts with Astrin and Regulates Astrin Levels to Promote Cell Division. Cell Rep 14(2):180–8. [PubMed: 26748699]

Grabarek Z. 2006. Structural basis for diversity of the EF-hand calcium-binding proteins. J Mol Biol 359(3):509–25. [PubMed: 16678204]

Hartman MA and Spudich JA. 2012. The myosin superfamily at a glance. J Cell Sci 125(Pt 7):1627–32. [PubMed: 22566666]

He K, Sakai T, Tsukasaki Y, Watanabe TM and Ikebe M. 2017. Myosin X is recruited to nascent focal adhesions at the leading edge and induces multi-cycle filopodial elongation. Sci Rep 7(1):13685. [PubMed: 29057977]

Heissler SM and Sellers JR. 2014. Myosin light chains: Teaching old dogs new tricks. Bioarchitecture 4(6):169–88. [PubMed: 26155737]

Heissler SM and Sellers JR. 2015. Four things to know about myosin light chains as reporters for non-muscle myosin-2 dynamics in live cells. Cytoskeleton (Hoboken) 72(2):65–70. [PubMed: 25712372]

Heissler SM and Sellers JR. 2016. Various Themes of Myosin Regulation. J Mol Biol 428(9 Pt B):1927–46. [PubMed: 26827725]

Homma K, Saito J, Ikebe R and Ikebe M. 2001. Motor function and regulation of myosin X. J Biol Chem 276(36):34348–54. [PubMed: 11457842]

Hunt SE, McLaren W, Gil L, Thormann A, Schuilenburg H, Sheppard D, Parton A, Armean IM, Trevanion SJ, Flicek P et al. 2018. Ensembl variation resources. Database (Oxford) 2018.

Hyrskyluoto A and Vartiainen MK. 2020. Regulation of nuclear actin dynamics in development and disease. Curr Opin Cell Biol 64:18–24. [PubMed: 32088545]

Jacquemet G, Hamidi H and Ivaska J. 2015. Filopodia in cell adhesion, 3D migration and cancer cell invasion. Curr Opin Cell Biol 36:23–31. [PubMed: 26186729]

Kerber ML and Cheney RE. 2011. Myosin-X: a MyTH-FERM myosin at the tips of filopodia. J Cell Sci 124(Pt 22):3733–41. [PubMed: 22124140]

Kerber ML, Jacobs DT, Campagnola L, Dunn BD, Yin T, Sousa AD, Quintero OA and Cheney RE. 2009. A novel form of motility in filopodia revealed by imaging myosin-X at the single-molecule level. Curr Biol 19(11):967–73. [PubMed: 19398338]

Kita AM, Swider ZT, Erofeev I, Halloran MC, Goryachev AB and Bement WM. 2019. Spindle-F-actin interactions in mitotic spindles in an intact vertebrate epithelium. Mol Biol Cell 30(14):1645–54. [PubMed: 31091161]

Kwon M, Bagonis M, Danuser G and Pellman D. 2015. Direct Microtubule-Binding by Myosin-10 Orients Centrosomes toward Retraction Fibers and Subcortical Actin Clouds. Dev Cell 34(3):323–37. [PubMed: 26235048]

Kwon M, Godinho SA, Chandhok NS, Ganem NJ, Azioune A, Thery M and Pellman D. 2008. Mechanisms to suppress multipolar divisions in cancer cells with extra centrosomes. Genes Dev 22(16):2189–203. [PubMed: 18662975]

Leijnse N, Oddershede LB and Bendix PM. 2015. An updated look at actin dynamics in filopodia. Cytoskeleton (Hoboken) 72(2):71–9. [PubMed: 25786787]

Li J, Lu Q and Zhang M. 2016. Structural Basis of Cargo Recognition by Unconventional Myosins in Cellular Trafficking. Traffic 17(8):822–38. [PubMed: 26842936]

Li Q and Sarna SK. 2009. Nuclear myosin II regulates the assembly of preinitiation complex for ICAM-1 gene transcription. Gastroenterology 137(3):1051–60, 60 e1–3. [PubMed: 19328794]

Li YR and Yang WX. 2016. Myosins as fundamental components during tumorigenesis: diverse and indispensable. Oncotarget 7(29):46785–812. [PubMed: 27121062]

Mogessie B and Schuh M. 2017. Actin protects mammalian eggs against chromosome segregation errors. Science 357(6353).

Morin X and Bellaiche Y. 2011. Mitotic spindle orientation in asymmetric and symmetric cell divisions during animal development. Dev Cell 21(1):102–19. [PubMed: 21763612]

Moujaber O and Stochaj U. 2020. The Cytoskeleton as Regulator of Cell Signaling Pathways. Trends Biochem Sci 45(2):96–107. [PubMed: 31812462]

Murthy K and Wadsworth P. 2005. Myosin-II-dependent localization and dynamics of F-actin during cytokinesis. Curr Biol 15(8):724–31. [PubMed: 15854904]

Nakajima YI. 2018. Mitotic spindle orientation in epithelial homeostasis and plasticity. J Biochem 164(4):277–84. [PubMed: 30020465]

Otto JJ, Kane RE and Bryan J. 1979. Formation of filopodia in coelomocytes: localization of fascin, a 58,000 dalton actin cross-linking protein. Cell 17(2):285–93. [PubMed: 378407]

Quintero OA and Yengo CM. 2012. Myosin X dimerization and its impact on cellular functions. Proc Natl Acad Sci U S A 109(43):17313–4. [PubMed: 23054838]

Rankin EB and Giaccia AJ. 2016. Hypoxic control of metastasis. Science 352(6282):175–80. [PubMed: 27124451]

Robinson DN and Spudich JA. 2000. Towards a molecular understanding of cytokinesis. Trends Cell Biol 10(6):228–37. [PubMed: 10802538]

Rogers MS and Strehler EE. 2001. The tumor-sensitive calmodulin-like protein is a specific light chain of human unconventional myosin X. J Biol Chem 276(15):12182–9. [PubMed: 11278607]

Sandquist JC, Larson ME and Hine KJ. 2016. Myosin-10 independently influences mitotic spindle structure and mitotic progression. Cytoskeleton (Hoboken) 73(7):351–64. [PubMed: 27220038]

Sato O, Jung HS, Komatsu S, Tsukasaki Y, Watanabe TM, Homma K and Ikebe M. 2017. Activated full-length myosin-X moves processively on filopodia with large steps toward diverse two-dimensional directions. Sci Rep 7:44237. [PubMed: 28287133]

Savci-Heijink CD, Halfwerk H, Koster J, Horlings HM and van de Vijver MJ. 2019. A specific gene expression signature for visceral organ metastasis in breast cancer. BMC Cancer 19(1):333. [PubMed: 30961553]

Sigrist CJ, De Castro E, Langendijk-Genevaux PS, Le Saux V, Bairoch A and Hulo N. 2005. ProRule: a new database containing functional and structural information on PROSITE profiles. Bioinformatics 21(21):4060–6. [PubMed: 16091411]

Sousa AD and Cheney RE. 2005. Myosin-X: a molecular motor at the cell's fingertips. Trends Cell Biol 15(10):533–9. [PubMed: 16140532]

Svitkina T. 2018. The Actin Cytoskeleton and Actin-Based Motility. Cold Spring Harb Perspect Biol 10(1).

Tang Z, Li C, Kang B, Gao G, Li C and Zhang Z. 2017. GEPIA: a web server for cancer and normal gene expression profiling and interactive analyses. Nucleic Acids Res 45(W1):W98–W102. [PubMed: 28407145]

Thery M and Bornens M. 2006. Cell shape and cell division. Curr Opin Cell Biol 18(6):648–57. [PubMed: 17046223]

Titus MA. 2018. Myosin-Driven Intracellular Transport. Cold Spring Harb Perspect Biol 10(3).

Tokuo H, Mabuchi K and Ikebe M. 2007. The motor activity of myosin-X promotes actin fiber convergence at the cell periphery to initiate filopodia formation. J Cell Biol 179(2):229–38. [PubMed: 17954606]

Tokuo H, Bhawan J and Coluccio LM. 2018. Myosin X is required for efficient melanoblast migration and melanoma initiation and metastasis. Sci Rep 8(1):10449. [PubMed: 29993000]

Torres JZ, Miller JJ and Jackson PK. 2009. High-throughput generation of tagged stable cell lines for proteomic analysis. Proteomics 9(10):2888–91. [PubMed: 19405035]

Torres JZ, Ban KH and Jackson PK. 2010. A Specific Form of Phospho Protein Phosphatase 2 Regulates Anaphase-promoting Complex/Cyclosome Association with Spindle Poles. Mol Biol Cell 21(6):897–904. [PubMed: 20089842]

Uraji J, Scheffler K and Schuh M. 2018. Functions of actin in mouse oocytes at a glance. J Cell Sci 131(22).

Vasquez CG, Heissler SM, Billington N, Sellers JR and Martin AC. 2016. Drosophila non-muscle myosin II motor activity determines the rate of tissue folding. Elife 5.

Walczak CE and Heald R. 2008. Mechanisms of mitotic spindle assembly and function. Int Rev Cytol 265:111–58. [PubMed: 18275887]

Weber KL, Sokac AM, Berg JS, Cheney RE and Bement WM. 2004. A microtubule-binding myosin required for nuclear anchoring and spindle assembly. Nature 431(7006):325–9. [PubMed: 15372037]

Woolner S, O'Brien LL, Wiese C and Bement WM. 2008. Myosin-10 and actin filaments are essential for mitotic spindle function. J Cell Biol 182(1):77–88. [PubMed: 18606852]

Wuhr M, Mitchison TJ and Field CM. 2008. Mitosis: new roles for myosin-X and actin at the spindle. Curr Biol 18(19):R912–4. [PubMed: 18957236]

Yu H, Chakravorty S, Song W and Ferenczi MA. 2016. Phosphorylation of the regulatory light chain of myosin in striated muscle: methodological perspectives. Eur Biophys J 45(8):779–805. [PubMed: 27084718]

Zhang L, Huang ST, Feng YL, Wan T, Gu HF, Xu J, Yuan LJ, Zhou Y, Yu XJ, Huang L et al. 2017. The Bidirectional Regulation between MYL5 and HIF-1alpha Promotes Cervical Carcinoma Metastasis. Theranostics 7(15):3768–80. [PubMed: 29109775]

Zhang YS, Liu B, Luo XJ, Li TB, Zhang JJ, Peng JJ, Zhang XJ, Ma QL, Hu CP, Li YJ et al. 2015. Nuclear cardiac myosin light chain 2 modulates NADPH oxidase 2 expression in myocardium: a novel function beyond muscle contraction. Basic Res Cardiol 110(4):38. [PubMed: 25982880]

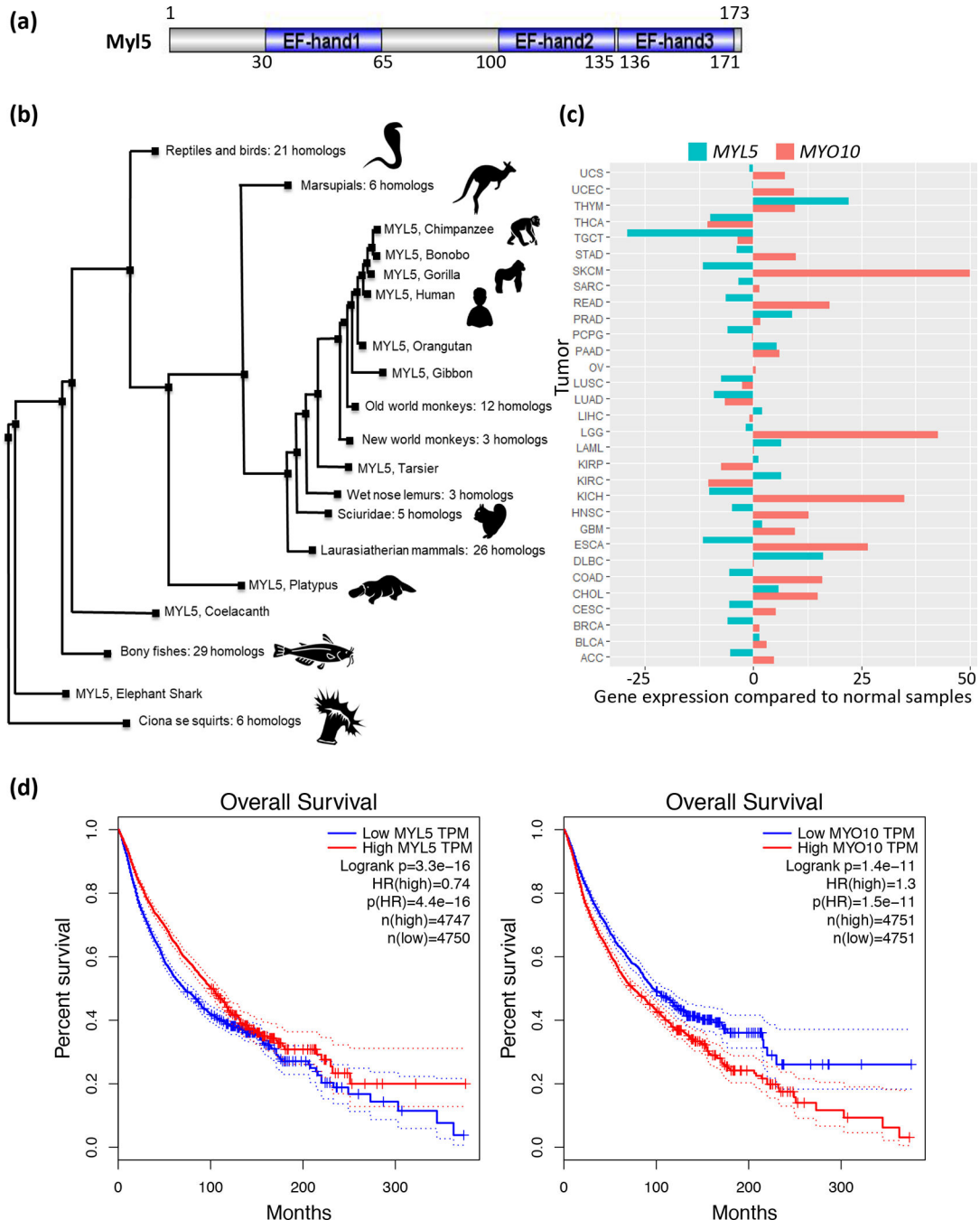

Figure 1.

In silico analyses of Myl5. (a) Schematic of the human Myl5 (UniProtKB-Q02045) protein domain architecture with the EF hand domains highlighted in blue. The number of amino acid residues are indicated. (b) Phylogenetic tree analysis showing that Myl5 is conserved among vertebrates. (c) Analysis of *MYL5* and *MYO10* differential gene expression in a broad array of cancers versus matched normal samples with the Gene Expression Profiling and Interactive Analysis (GEPIA) web server. See Table S2 for a list of cancer types considered and their corresponding abbreviations. The median gene expression levels are on

the x-axis and cancer type is on the y-axis. Positive values represent higher gene expression in tumor samples compared to normal samples and negative values represent lower gene expression in tumor samples compared to normal samples. (d) Correlation analysis between *MYL5* and *MYO10* mRNA levels and the overall survival of cancer patients using the GEPIA web server. Survival plots indicate time in months on the x-axis and percent survival on the y-axis. See materials and methods for analysis details.

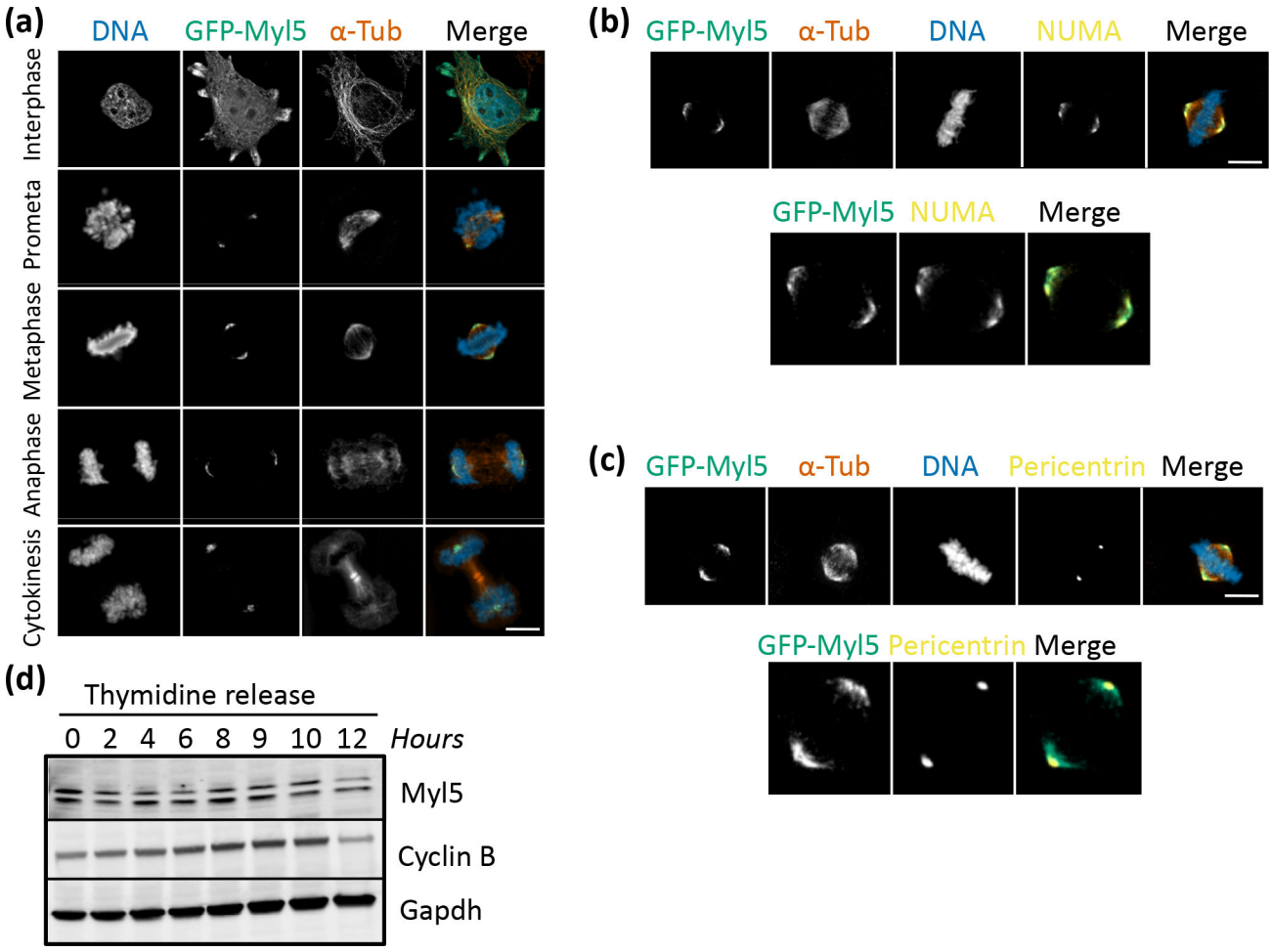

Figure 2.

Myl5 localizes to mitotic spindle poles during mitosis. (a) The LAP (GFP-TEV-S-Peptide)-tagged-Myl5 HeLa inducible stable cell line was treated with Dox for 16 hours to express GFP-Myl5 and cells were fixed, stained with Hoechst 33342 DNA dye, and anti-α-Tubulin and anti-GFP antibodies and imaged by immunofluorescence microscopy. Images show the cell cycle subcellular localization of GFP-Myl5 during interphase, prometaphase, metaphase, anaphase and cytokinesis. Bar indicates 5μm. (b-c) Same as in (a), except that cells were also stained with anti-NUMA (b) or anti-Pericentrin (c) antibodies. Bar indicates 5μm. (d) Analysis of endogenous Myl5 protein levels throughout the cell cycle. HeLa cells were synchronized in G1/S, released into the cell cycle and cells were harvested at the indicated time points. Protein extracts were prepared, resolved by SDS-PAGE, transferred to a PVDF membrane and immunoblotted with the indicated antibodies. Gapdh is used a loading control.

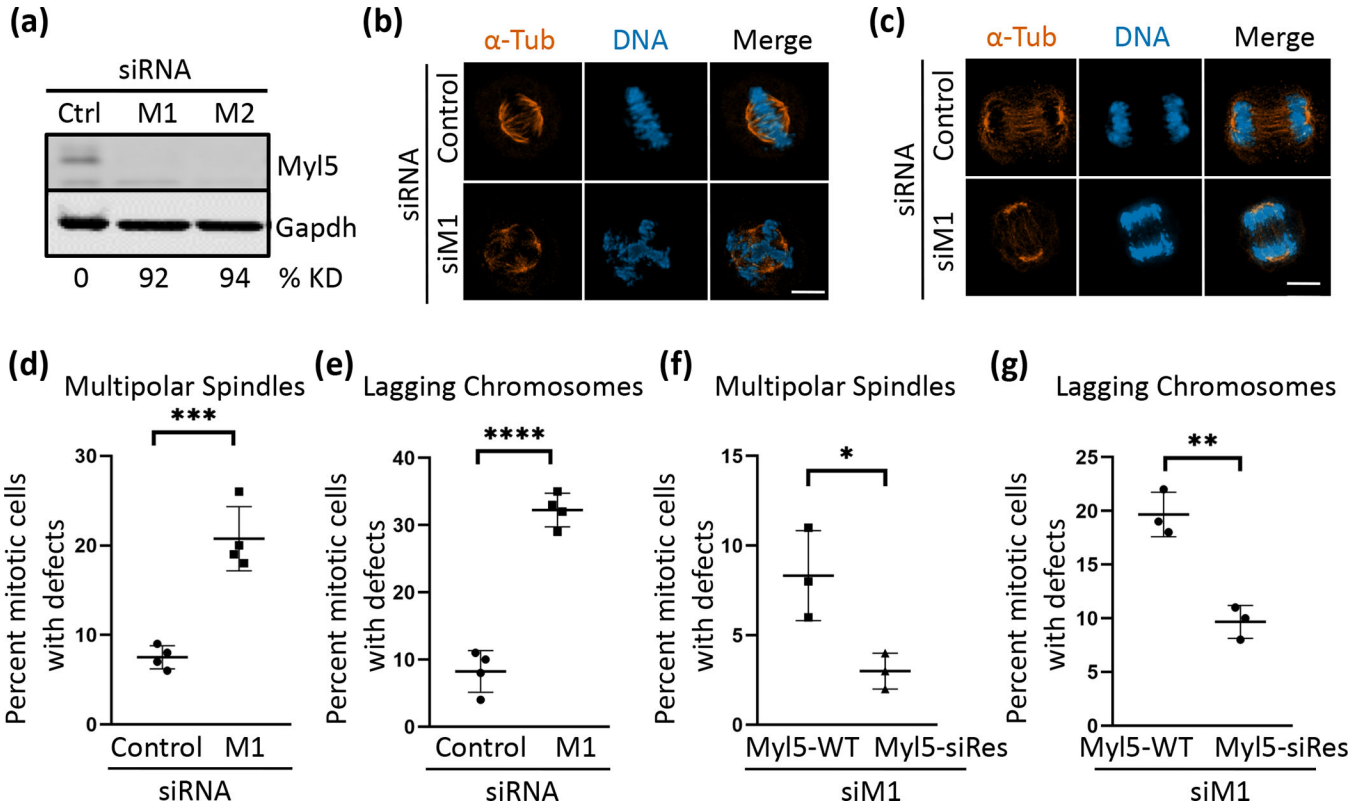

Figure 3.

Depletion of Myl5 leads to spindle assembly and cell division defects. (a) Immunoblot analysis showing that siRNA oligonucleotides targeting *MYL5* (M1 and M2) expression deplete Myl5 protein levels in HeLa cells compared to non-targeting control siRNA (siCtrl). Percent Myl5 protein level knockdown (% KD) normalized to Gapdh is indicated for each oligonucleotide. (b-c) Immunofluorescence microscopy of HeLa cells transfected with siCtrl or siM1 for 72 hours, fixed, and stained with Hoechst 33342 DNA dye and anti-α-Tubulin antibodies. Scale bar indicates 5μm. (d-e) Quantitation of the percent mitotic cells with multipolar spindles (d) and lagging chromosomes (e) in siCtrl or siM1 transfected cells. Data represent the average ± SD of four independent experiments, 100 cells counted for each. *** indicates a p value =.0004 and **** a p value <.0001. (f-g) The LAP-Myl5-WT and LAP-Myl5-siRes (resistant to siM1 siRNA targeting Myl5) HeLa inducible stable cell lines were transfected with siM1 for 46 hours, synchronized in G1/S with thymidine for 18 hours, released into the cell cycle for 8 hours, and induced with Dox during the last 16 hours of the experiment to overexpress either GFP-Myl5-WT or GFP-Myl5-siRes. Cells were then fixed and analyzed by immunofluorescence microscopy and the percent mitotic cells with mitotic defects (multipolar spindles (f) and lagging chromosomes (g)) was quantified. Data represent the average ± SD of three independent experiments, 100 cells counted for each. ** indicates a p value =.0026 and * indicates a p value =.0270.

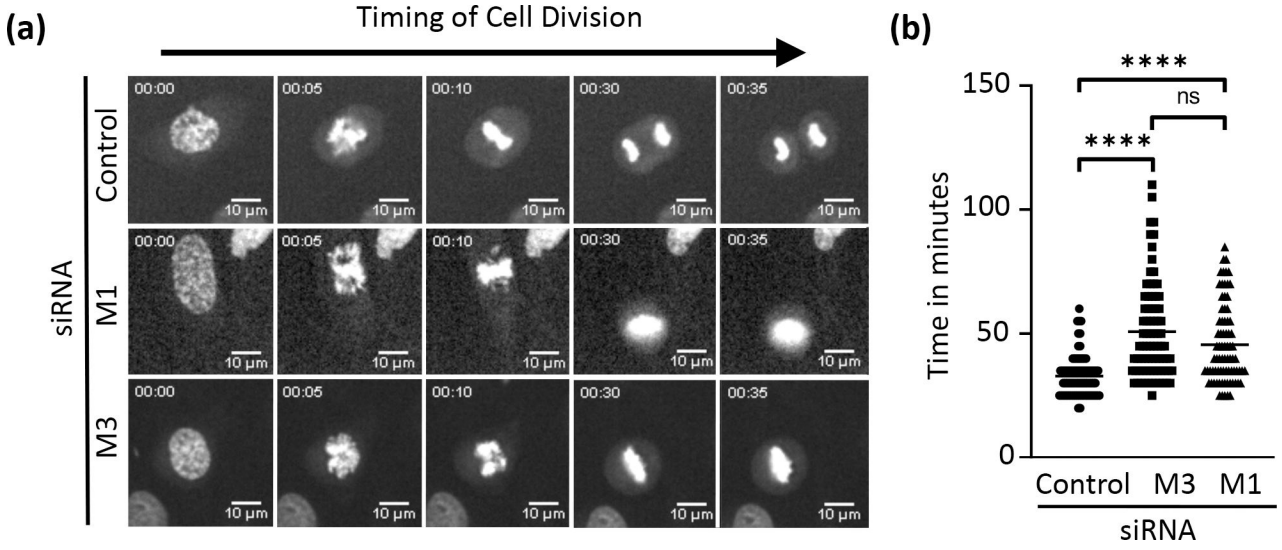

Figure 4.

Modulation of Myl5 levels affects the time to cell division. (a) Live-cell time-lapse microscopy of HeLa cells transfected with siCtrl or siM1 or siM3 for 72 hours. Cells were then synchronized in G1/S with thymidine treatment for 18 hours, released, and imaged by staining the cells with SiR-DNA stain at five hours post-release. The indicated times are in minutes. See Videos S1–S3. (b) Quantitation of the time cells spend in mitosis from DNA condensation to chromosome separation. Y-axis indicates time in minutes. X-axis indicates the siRNA transfections. Data represent the average ± SD of three independent experiments, 30 cells counted for each. **** indicates p value <.0001.

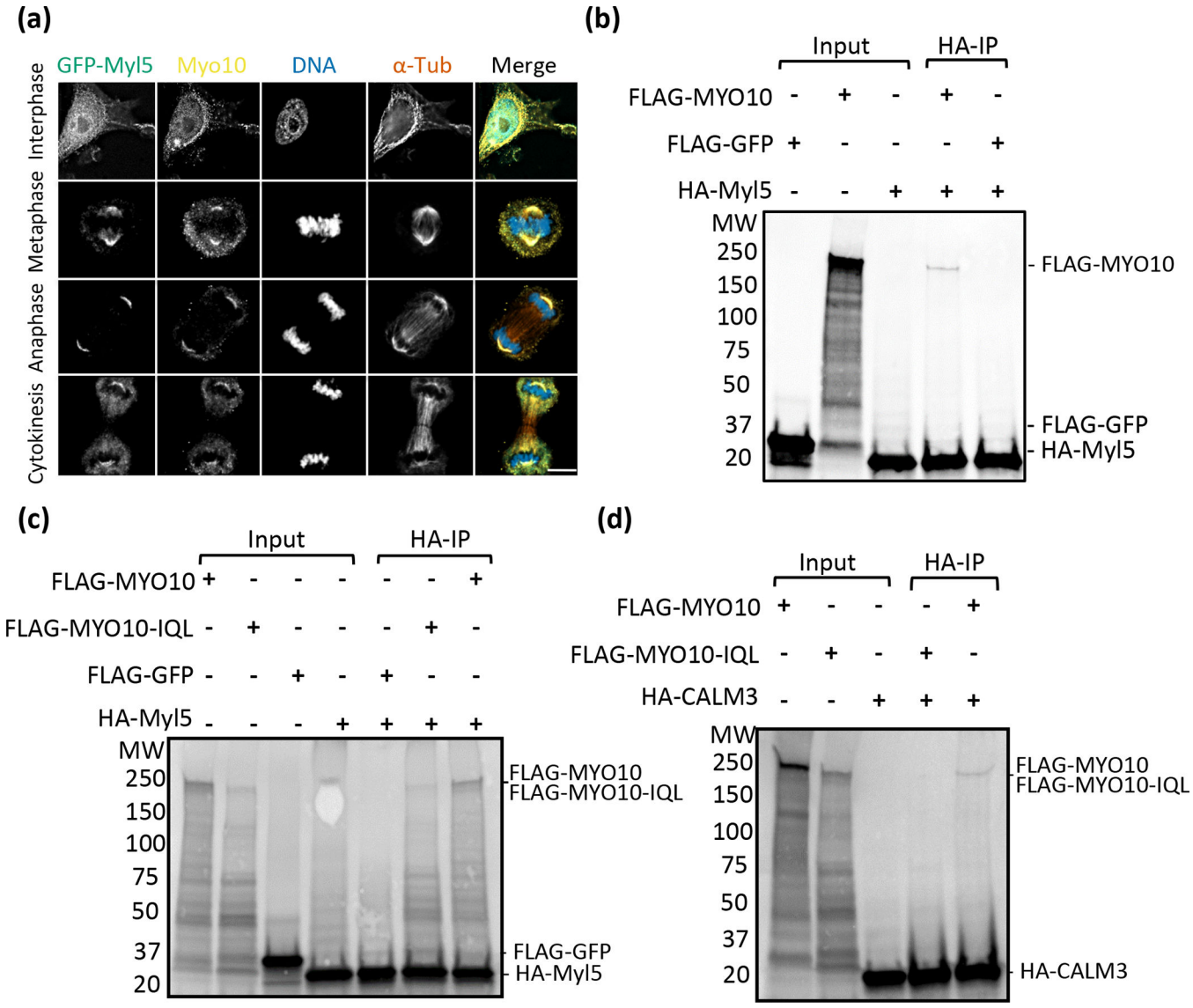

Figure 5.

Myl5 colocalizes with MYO10 at mitotic spindle poles during mitosis and binds to MYO10 *in vitro*. (a) The LAP (GFP-TEV-S-Peptide)-tagged-Myl5 HeLa inducible stable cell line was treated with Dox for 16 hours to express GFP-Myl5 and cells were fixed, stained with Hoechst 33342 DNA dye, and anti-α-Tubulin and anti-MYO10 antibodies and imaged by immunofluorescence microscopy. Images show the cell cycle subcellular localization of GFP-Myl5 and MYO10 during interphase, metaphase, anaphase and cytokinesis. Bar indicates 5μm. (b) *In vitro* binding assays performed in the presence or absence of radiolabeled (^{35}S methionine) FLAG-MYO10, FLAG-GFP, or HA-Myl5. HA-Myl5 was immunoprecipitated (IP) and eluates were analyzed by radiometry. See materials and methods for experimental details. (c) Same as in (b), except that FLAG-MYO10-IQL (MYO10 IQ-less mutant) was added to the analysis. (d) Same as in (c), except that the binding of HA-CALM3 to FLAG-MYO10 or FLAG-MYO10-IQL was analyzed instead of

HA-Myl5. See Figure S4 for control experiment showing that FLAG-MYO10 and FLAG-MYO10-IQL do not bind non-specifically to anti-HA beads.

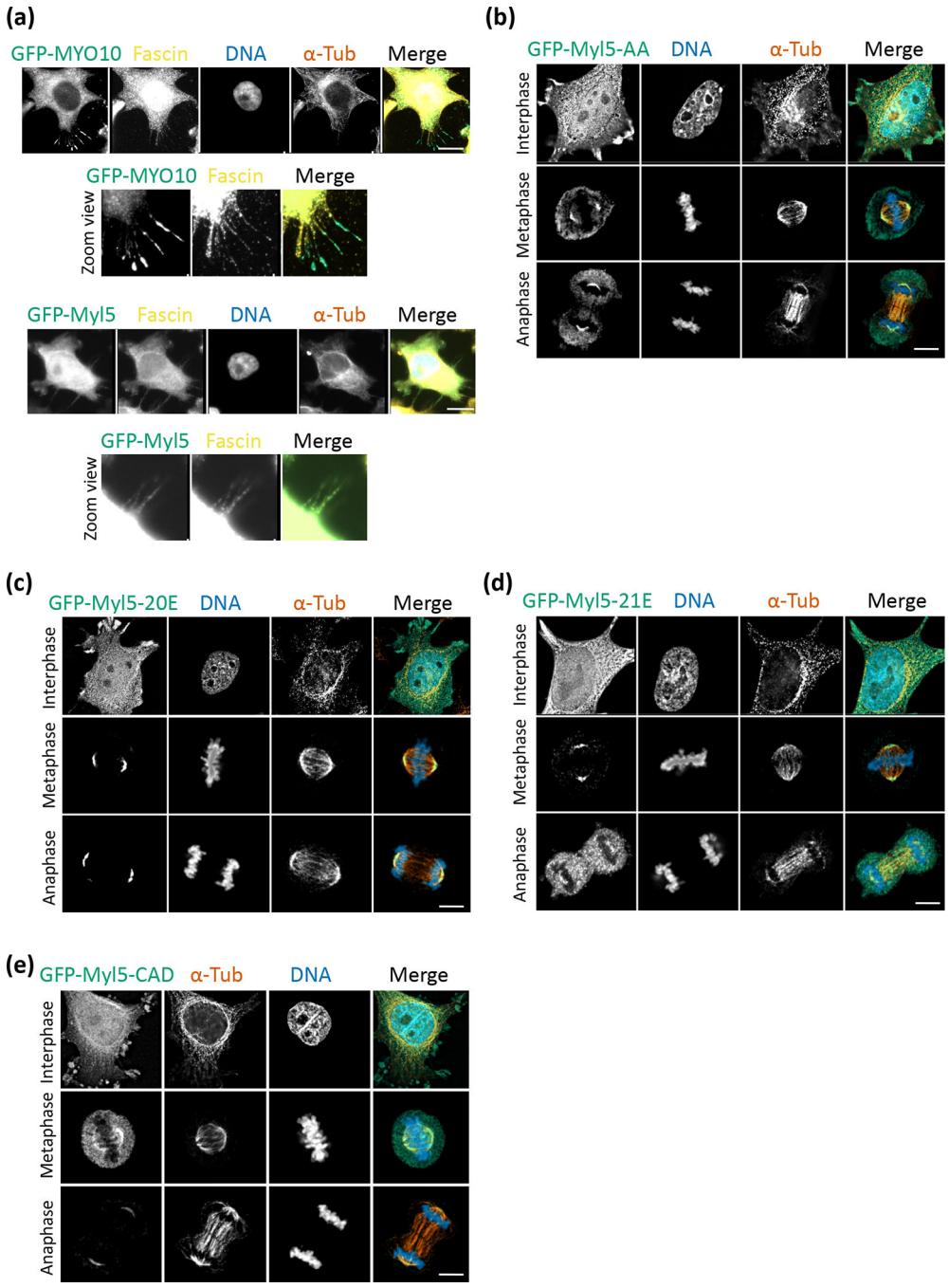

Figure 6.

Myl5 localizes to the leading edge and filopodia. (a) The LAP (GFP-TEV-S-Peptide)-tagged-Myl5 or MYO10 HeLa inducible stable cell lines were treated with Dox for 16 hours to express GFP-Myl5 or GFP-MYO10 and cells were fixed, stained with Hoechst 33342 DNA dye, anti-GFP and anti-α-Tubulin, and anti-Fascin (filopodia marker) antibodies, and imaged by immunofluorescence (IF) microscopy. Bars indicate 5μm. Bottom panels of GFP-Myl5 and GFP-MYO10 IF images show magnified view of filopodia. (b-e) GFP-Myl5-AA (phospho-null), GFP-Myl5-20E and GFP-Myl5-21E (phospho-mimics), and GFP-Myl5-

CAD (calcium-binding domain deletion) mutants were expressed in HeLa cells for 16 hours and cells were fixed, stained with Hoechst 33342 DNA dye, and anti-α-Tubulin and anti-GFP antibodies and imaged by IF microscopy. Bars indicate 5μm.